EPJ manuscript No.
(will be inserted by the editor)

Neuronal Excitability Level Transition Induced by Electrical Stimulation

Gerson Florence[1,2,3,4,a], Jürgen Kurths[3,4], Birajara Soares Machado[5], Erich Talamoni Fonoff[2], Hilda Alicia Cerdeira[6], Manoel Jacobsen Teixeira[2], and Koichi Sameshima[1]

[1] Dept. Radiology & Oncology, LIM/43, School of Medicine, University of São Paulo, São Paulo, Brazil
[2] Dept. Neurology, LIM/26, School of Medicine, University of São Paulo, São Paulo, Brazil
[3] Institute of Physics, Humboldt University, Berlin, Germany
[4] Potsdam Institute for Climate Impact Research, Potsdam, Germany
[5] Brain Institute, Hospital Israelita Albert Einstein, São Paulo, Brazil
[6] Instituto de Física Teórica, UNESP - Universidade Estadual Paulista, São Paulo, Brazil.

Abstract. In experimental studies, the electrical stimulation (ES) has been applied to induce neuronal activity or to disrupt pathological patterns. Nevertheless, the underlying mechanisms of these activity pattern transitions are not clear. To study these phenomena, we simulated a model of the hippocampal region CA1. The computational simulations using different amplitude levels and duration of ES revealed three states of neuronal excitability: burst-firing mode, depolarization block and spreading depression wave. We used the bifurcation theory to analyse the interference of ES in the cellular excitability and the neuronal dynamics. Understanding this process would help to improve the ES techniques to control some neurological disorders.

1 Introduction

The neuronal electrical activity can be changed by an abnormal increase of cellular excitability, which happens in some neurological disorders. In Parkinson's disease (PD), the discharge pattern of subthalamic nucleus presents a mixed burst-firing mode [1]. In epilepsy, the epileptogenic zone presents a stereotyped neuronal activity characterized by a paroxysmal depolarizing shift (high amplitude of depolarization, 20–40 mV) with 50–200 ms duration that triggers a burst of spikes [2]. Furthermore, brief interruptions in population spike activity can be detected during an epileptic seizure [3]. This spike inhibition is derived from highly depolarized state of the basal membrane potential (around -40 mV), the so-called depolarization block (DB) [4]. DB is also observed in dopaminergic neurons after repeated administration of antipsychotic drugs to rats. Some authors argue that this phenomenon may be associated to antipsychotic medication efficacy in schizophrenia patients [5-7]. Another phenomenon is the spreading depression (SD) that has been associated to migraine preceded by aura (sensory hallucinations). SD is characterized by a slow depolarizing wave that lasts

[a] e-mail: geflorence@gmail.com

for around 1 min. In this case, the membrane potential shifts toward zero. Similarly for DB, there is an action potential inactivation [2].

The electrical stimulation (ES) protocols have been applied either to induce neuronal activity or to disrupt pathological electrical activity patterns. In experimental studies, ES can trigger epileptiform discharges [8,9], whose protocol was reproduced in computational models of the hippocampus to understand the underlying mechanisms of neuronal epileptiform activity [10,11]. Nevertheless, ES can also interrupt epileptic seizures [12]. Likewise this method is used successfully in the treatment of movement disorders and neuropsychiatric diseases, e.g., depression, obsessive-compulsive disorder and addiction. In this procedure, the so-called deep brain stimulation (DBS), the electrical current is delivered into the brain parenchyma through chronically implanted electrodes. The DBS therapeutic effects depend on the location of implanted electrodes and ES parameters (current amplitude, pulse width and frequency) [1].

Computational models have been explored to study abnormal patterns in Parkinsons disease [13,14], epilepsy [2,11], neuropsychiatric diseases [15,16], depolarization block and spreading depression phenomena [2,17,18]. Moreover, the bifurcation theory has been applied to analyse the dynamics of neuronal behaviour, varying some parameters that change the cellular excitability [19]. However, the underlying mechanisms of these activity pattern transitions (burst-firing mode, depolarization block and spreading depression) and how ES interferes with this process are not completely understood. To study these phenomena, we simulated a model of the hippocampal region CA1 with different levels of ES amplitude and time period, and analysed the neuronal dynamics based on bifurcation theory. Understanding the underlying mechanisms of the transitions to different states of cellular excitability will help to develop more efficient ES control of some neurological diseases.

2 Methods

We used a modified version of the Golomb model [2] in the computational simulations. This is a somatic single-compartment model of the hippocampal region CA1. The ionic currents of the soma and of proximal dendrites are transient Na^+ current, $I_{Na} = G_{Na}(V - E_{Na})$ with $G_{Na} = g_{Na}m^3h$, persistent sodium current, $I_{NaP} = G_{NaP}(V - E_{Na})$ with $G_{NaP} = g_{NaP}p$, delayed rectifier K^+ current, $I_{Kdr} = G_{Kdr}(V - E_K)$ with $G_{Kdr} = g_{Kdr}n^4$, muscarinic-sensitive K^+ current, $I_{Km} = G_{Km}(V - E_K)$ with $G_{Km} = g_m z$, A-type K^+ current, $I_{KA} = G_{KA}(V - E_K)$ with $G_{KA} = g_A a^3 b$, and leak current, $I_L = g_L(V - V_L)$ with $g_L = 0.17$ mS/cm^2 and $V_L = -66$ mV. The variable V is the membrane potential, E_K and E_{Na} are the potassium and sodium Nernst potentials, $E_{ion} = 58\log([ion]_o/[ion]_i)$, respectively. The voltage-sensitive channels are m, h, p, n, z, a and b [20]. The Golomb model equations and the simulation codes can be accessed in the ModelDB databases.[1] Other currents were added, e.g., pump current, Na^+ and K^+ leak currents, $I_{LX} = g_{LX}(V - E_X)$, $X = \{Na, K\}$, $g_{LNa} = 0.0269$ mS/cm^2, and $g_{LK} = 0.0837$ mS/cm^2 that determine the membrane potential in the resting state.

This modified model included intra- and extracellular spaces, $Na^+ - K^+$ pump, glial-buffer, ion diffusion, and K^+ and Na^+ ionic concentrations [10,11,18,21]. These mechanisms regulated the extracellular potassium concentration (Fig. 1),

[1] https://senselab.med.yale.edu/modeldb/ShowModel.asp?Model= 66268

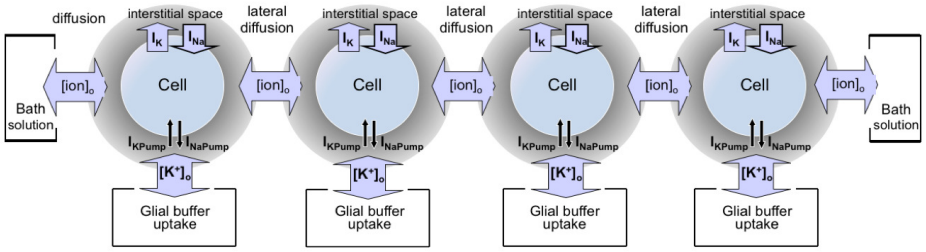

Fig. 1. Schematic diagram based on the model proposed by Park and Durand [10]

$$\begin{aligned} A_{pump} &= (1 + Km_K/[K^+]_o)^{-2}(1 + Km_{Na}/[Na^+]_i)^{-3} \ , \\ I_{Kpump} &= -2I_{max}A_{pump} \ , \\ I_{Napump} &= 3I_{max}A_{pump} \ , \\ I_{pump} &= I_{Napump} + I_{Kpump} \ , \end{aligned} \tag{1}$$

where $[K^+]_o$ and $[Na^+]_i$ are the total extracellular potassium concentration and the total intracellular sodium concentration, respectively. $I_{max}(= 20\ \mu\text{A/cm}^2)$ is the maximal current generated by the pump, while $Km_K = 2$ mM/l and $Km_{Na} = 10$ mM/l [18]. For the glial potassium regulation and ion diffusion, we used simplified models, the glial-buffering equations [18,21],

$$\begin{aligned} \frac{d[B]_o}{dt} &= [K^+]_{glial\text{-}buffering} \ , \\ [K^+]_{glial\text{-}buffering} &= k_1([B]_{max} - [B]_o) - k_2[K^+]_o \ , \\ k_2 &= 0.0008/(1 + \exp(([K^+]_o - 15)/-1.09)) \ , \end{aligned} \tag{2}$$

where $[B]_o$ is the free buffer extracellular concentration, $[B]_{max} = 265$ mM/l is the total buffer capacity, and $[K^+]_{glial\text{-}buffering}$ is the potassium concentration removed by glial cell from extracellular space, while $k_1 = 0.0008$ is a rate constant. We used the lateral ion diffusion proposed by Park and Durand [10] (see Fig. 1),

$$[ion]_{lateral\ diffusion} = -([ion]_o - [ion]_L)/\tau_{SS} \ . \tag{3}$$

$[K^+]_{lateral\ diffusion}$ and $[Na^+]_{lateral\ diffusion}$ are extracellular ion concentrations originated from adjacent cells (lateral diffusion) and from the bath solution. $[ion]_L$ is the extracellular ion concentration of the adjacent cells, and $\tau_{ss} = 20$ ms is a time constant. Specifically in K^+ diffusion from the bath solution to the cell, we used $\tau_{bs} = 30 \times 10^3$ ms to reduce the influence of the bath solution. It absorbs K^+ from the extracellular space, limiting the increase of $[K^+]_o$ during neuronal activity. Here, in the one dimensional network, the first and last cells are embedded in a bath solution with $[K^+]_{bath}$ (3.5 mM/l) and $[Na^+]_{bath}$ (140 mM/l) and the other cells between them are only coupled by ion lateral diffusion [10]. Then, the total extracellular and intracellular ion concentrations can be expressed by the following equations:

$$\begin{aligned}
\frac{[K^+]_o}{dt} &= [K^+]_{glial\text{-}buffering} + [K^+]_{lateral\ diffusion} + [K^+]_{bath\ diffusion} + [K^+]_{o(currents)}\ , \\
\frac{[Na^+]_o}{dt} &= [Na^+]_{lateral\ diffusion} + [Na^+]_{bath\ diffusion} + [Na^+]_{o(\ currents)}\ , \\
\frac{d[K^+]_i}{dt} &= [K^+]_{i(currents)}\ , \\
\frac{d[Na^+]_i}{dt} &= [Na^+]_{i(currents)}\ .
\end{aligned} \tag{4}$$

$[ion]_{i(currents)}$ is the ion concentration produced by Na^+, K^+ and pump currents during neuronal activity:

$$\begin{aligned}
[ion]_{i(currents)} &= (I_{\Sigma(ion)} 10^{-3} Area)/(F\, Vol_i)\ , \\
[ion]_{o(currents)} &= -\,(I_{\Sigma(ion)} 10^{-3} Area)/(F\, Vol_o)\ .
\end{aligned} \tag{5}$$

Here, $I_{\Sigma(ion)}$ is the total ion current (A/cm^2, multiplied by 10^{-3} to convert to milliseconds). $F = 96.49$ C/mMol is the Faraday constant, Vol_i is the soma volume and the extracellular volume is $Vol_o = rv.Vol_i$, and $rv = 0.15$ is the volume ratio [18].The simulations were implemented in Matlab R2009b (The MathWorks, Natick, MA). The bifurcation diagram was calculated by using the software XPP-AUTO.

3 Results

Using different time period of stimulation and varying amplitude levels of the direct current, the computational simulations showed three stages of neuronal excitability: burst-firing mode, depolarization block (DB) and SD wave.

3.1 Burst-firing mode

In Fig. 2, the ES triggered a sequence of action potentials (APs). The APs leaded to a continuous growth of extracellular potassium concentration ($[K^+]_o$). It is well known that increasing $[K^+]_o$ reduces the K^+ flow out of the cell due to decreasing of the difference in the K^+ concentrations between the two sides of the membrane [22,23]. Thus, the continuous growth of $[K^+]_o$ provoked a depression of K^+ currents (Fig. 3). The ES and depressed K^+ currents kept the membrane potential at a high level, impairing the cellular repolarisation process. Therefore, there was a gradual increase in the burst duration following $[K^+]_o$ increase. During the ES, the glial-buffering capacity was not compromised, since there was a low variation of the free buffer extracellular concentration.

3.2 Depolarization block (DB)

Increasing the period of ES the following burst mode shifted to the DB state (Fig. 4a). At this stage, the continuous increase of extracellular potassium concentration during ES overcame the ability of cellular mechanisms to restore the normal ionic concentrations levels. This impairment in ionic homeostasis is shown in the Fig. 4b. Differently

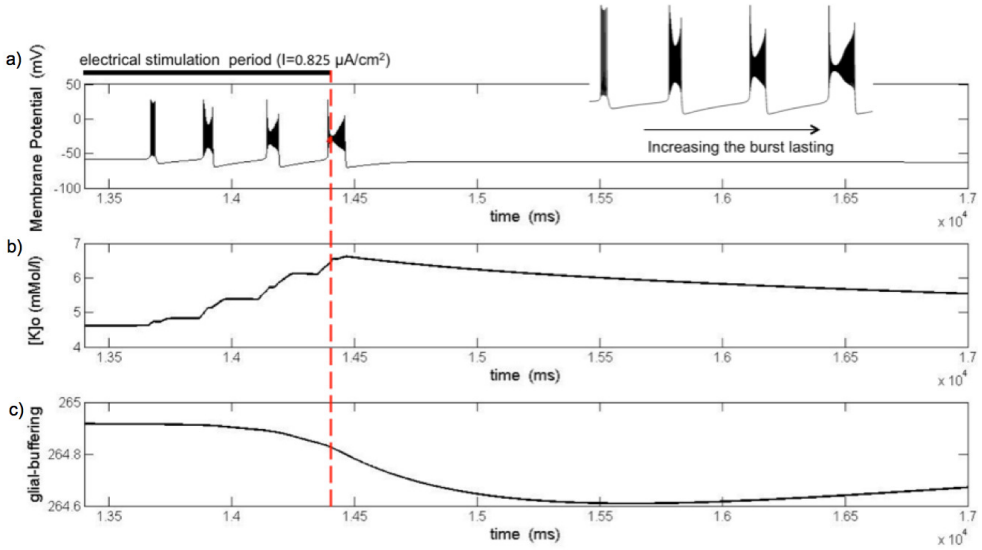

Fig. 2. Effects of direct current (I_D=0.825 μA/cm^2) stimulation on membrane potential, $[K^+]_o$ and glial-buffering ($[B]_o$ - free buffer extracellular concentration) during the burst-firing mode.

from the previous simulation (Fig. 2), after the ES interruption the free buffer extracellular concentration did not recover the glial-buffering capability. Thus, at high $[K^+]_o$ (around 10 mM/l) there was a depolarization shift of the membrane potential which results in an action potential (AP) blockage. The depolarization block (DB) process is illustrated in Fig. 5a. Within high $[K^+]_o$ condition, there was an unbalance between the excitatory and inhibitory currents. Fig. 5b shows the consequences of this unbalance in ionic current dynamics. In this case, the depressed K^+ currents caused by high $[K^+]_o$ could not reduce the level of the membrane potential after each AP in opposition to Na^+ currents. Herewith, a new spiking would be initiated when the K^+ conductance was still high (decreasing the AP amplitude). This process will continue until the AP inactivation occurs [2]. Afterwards, a low oscillation could be erupted. The slow activation of some potassium currents (e.g., muscarinic-sensitive K^+ current) may diminish the level of the membrane potential creating the condition to the oscillatory behaviour (Fig. 4a).

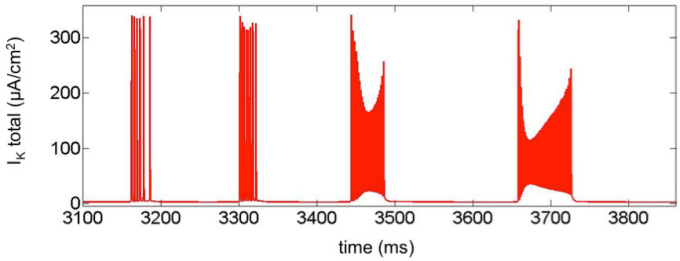

Fig. 3. The depression of K^+ currents over the time ($I_K total = I_{Kdr} + I_{Km} + I_{KA} + I_{KL}$). The direct current used in this simulation was I_D=1.5 μA/cm^2.

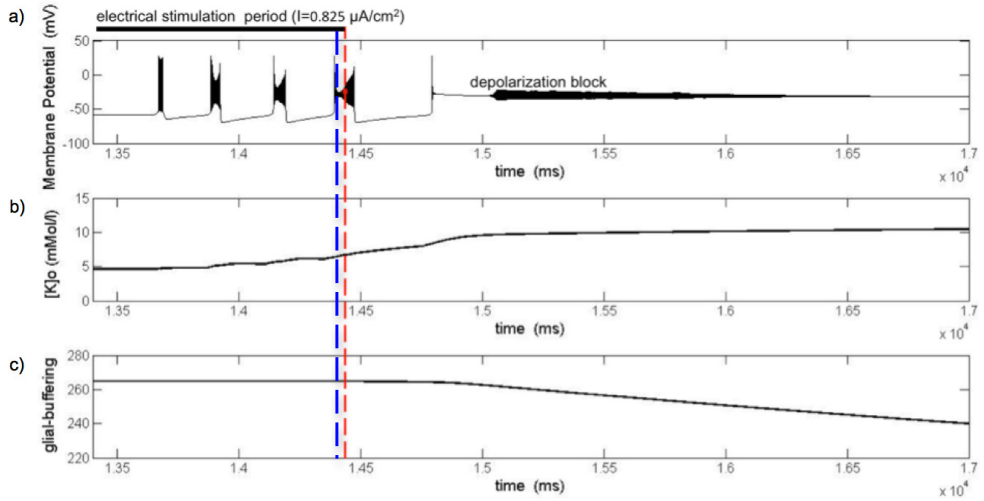

Fig. 4. Effects of direct current (I_D=0.825 μA/cm^2) stimulation on membrane potential, $[K^+]_o$ and glial-buffering ($[B]_o$ - free buffer extracellular concentration) during depolarization block. The first and second dotted lines show when the ES stops in the simulations presented in Fig. 2 and here, respectively.

Another important ES parameter is the direct current (I_D) amplitude. With the I_D increase, the DB state begins earlier. These effects on the neuronal dynamics are shown in Fig. 6. The amplitude of I_D applied to an isolated neuron was considered as a parameter in the bifurcation analysis. In this case, the K^+ diffusion between cells was not considered. Herewith, higher ES intensity was necessary to activate the neuron (isolated neuron: $I_D = 1.222$ μ A/cm^2; and neural network: $I_D = 0.8133$ μA/cm^2). Other cellular mechanisms (e.g., the synaptic transmission), not considered here, can also influence the effects of selected ES parameter. Varying ES amplitude, different stages of neuronal excitation could be observed. Low ES did not produce any changes in cell excitability. This state of the membrane resting equilibrium is represented by the stable branch of bifurcation diagram. The system lost the stability (unstable branch), when I_D initially induced APs. However, higher ES can immediately produce a burst mode followed by DB state. After a supercritical Andronov-Hopf bifurcation (Fig. 6b), the system evolved to a stable state at an elevated level of membrane depolarization. Moreover, depending on how high ES is, DB may occur without gradual reduction in the AP amplitude.

3.3 SD wave

The transition to SD showed some similarities with the depolarization block (Fig. 7). Nevertheless, after the AP inactivation process and decreasing glial capacity of K^+ uptake, the Na^+ currents overcame the K^+ currents, producing a positive net current which would slowly depolarize the membrane potential from -34 mV near to zero (Fig. 7a). During this process, the SD was maintained by a positive feedback between raising $[K^+]_o$ and membrane depolarization (Fig. 7b). The large increase of $[K^+]_o$ was essential to the continuation of the slow depolarization process, since there was a significant augment of K^+ conductance (G_{Kdr}) (Fig. 8). In the SD state, there was a net depolarization current, but in DB this phenomenon did not happen. Moreover, increasing the amplitude of ES produced a faster transition from bursting to DB and

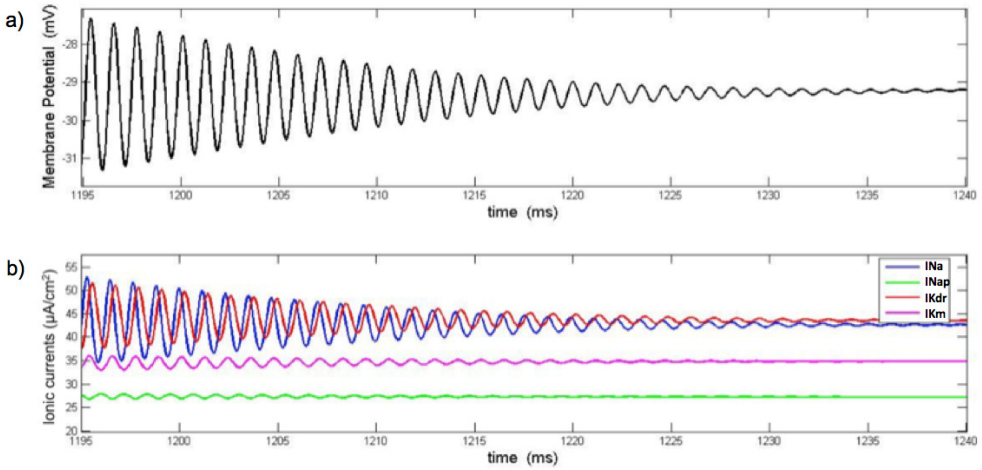

Fig. 5. The depolarization block process (DB). a) Membrane potential during the gradual AP reduction until the complete inactivation. b) Ionic currents oscillations. The interplay between I_{Kdr} and I_{Na} determines the AP behaviour. Decreasing I_{Kdr} due to high $[K^+]_o$ impaired the membrane repolarisation, keeping it at an elevated state of depolarization. The K^+ ionic current presents negative values, but it was shown here as absolute values to facilitate the comparison with the Na^+ current oscillation. The direct current used in this simulation was I_D=1.8 μA/cm^2.

from DB to SD. The glial capacity of K^+ uptake influenced the transition between these three different stages. Particularly the transition to SD is marked by a strong depletion of glial-buffering (Fig. 7c).

4 Discussion

Our computational simulation results are consistent with the experimental evidences of neuronal excitability increase concomitant to extracellular K^+ growth and its association with the transition to burst-firing mode, depolarization block (DB) and SD wave [3,9]. In the performed simulations, these transitions to different neuronal excitability levels were induced by changing either ES amplitude or duration. The direct current triggered an intense neuronal activity, which produced potassium accumulation in extracellular space. This ionic accumulation provoked a depression of potassium currents. Therewith, there was an increase in the burst duration due to the difficulty of these currents to repolarise the cell membrane. Increasing the amplitude or duration of stimulation, the K^+ accumulation reached a high $[K^+]_o$ leading to AP inactivation. However, the ionic channels continued partially open, keeping the high $[K^+]_o$ during DB state. As shown in Fig. 7, this situation changed when there was a strong reduction of glial-buffer capability. At this moment, the neuronal activity transited to SD wave. This wave is characterized by a slow depolarisation associated to a significant increase in extracellular potassium [24]. Despite the K^+ higher conductance than Na^+'s along the SD wave (Fig. 8), the elevated $[K^+]_o$ reduced the potassium currents sufficiently to produce a positive net current that slowly depolarized the cell membrane. Therefore, these simulations suggest that the different levels of potassium concentrations could be an important factor in the control of cellular excitability within some patterns of neuronal activity. However, other cellular mecha-

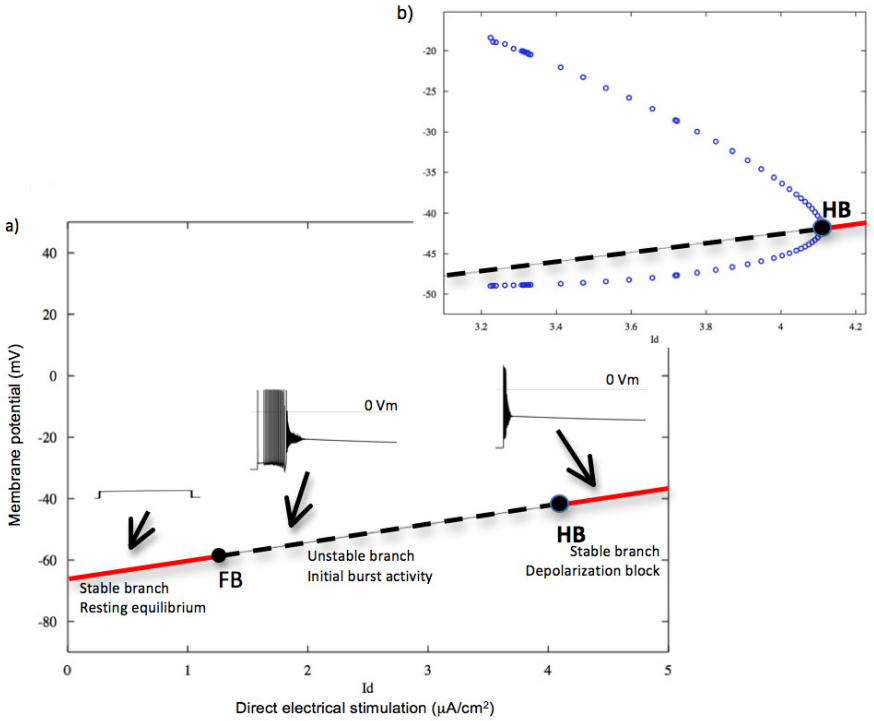

Fig. 6. Bifurcation diagram of V versus I_D. a) Red line and black dotted line refer to stable and unstable equilibria, respectively. FB is the fold bifurcation and HB is the Hopf bifurcation. b) Zoom of supercritical Andronov-Hopf bifurcation at higher amplitude of I_D.

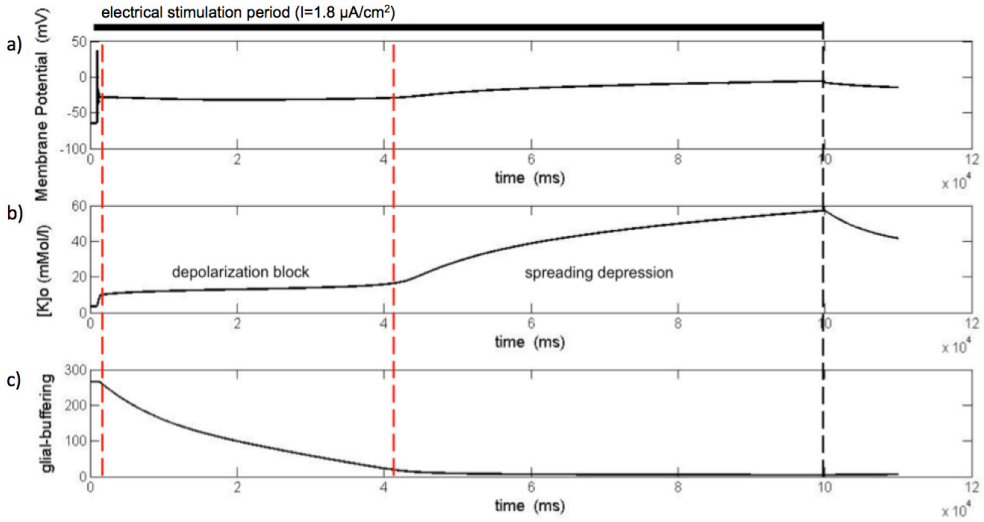

Fig. 7. Effects of direct current ($I_D = 1.8$ A/cm^2) stimulation on membrane potential, $[K^+]_o$ and glial-buffering during spreading depression wave.

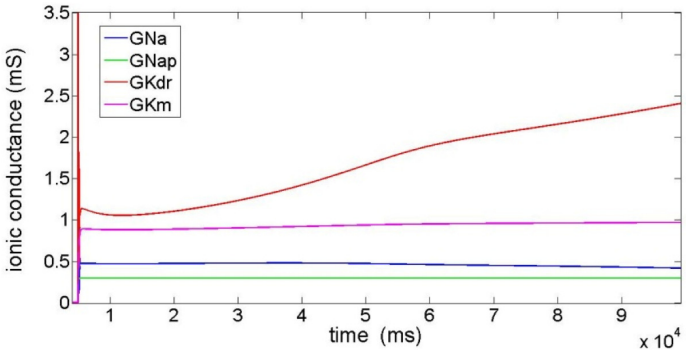

Fig. 8. Conductance variations during SD (I_D=1.8 μA/cm^2).

nisms could be implicated during ES, such as different types of synaptic transmission [25].

The potassium influence on neuronal behaviour is not a new idea [26,27], and some authors have debated the potassium role from a dynamical systems point of view [23,28,29]. One type of epileptic seizure – the tonic-clonic seizure – was analysed as a bistable state (coexistence of two oscillatory modes) with hysteresis between tonic firing and bursting at high $[K^+]_o$ [30]. Another study showed that a dopaminergic neuron model could exhibit bistability between tonic firing and depolarization block state [31]. Our simulations showed that this type of bistability may occur depending on the amplitude of electrical stimulation. In a computational simulation of hippocampus model, the neuronal synchronization could be induced by potassium diffusion through the interstitial space between adjacent neurons [10]. Moreover, the diffusion of high potassium concentration may lead the system to lose its stability and trigger an intense and long-lasting seizure-like activity in the neural circuit. In this case, Na^+K^+ pump could play a key role in the modulation of neuronal activity within a condition of depressed potassium currents due to high $[K^+]_o$ [2]. The glial-buffering is also an important mechanism of potassium regulation [32-34]. A bifurcation analysis has shown that reducing the levels of glial-buffering may induce cellular membrane to the depolarization block state [17]. This important role of glial cell was also observed in our analysis. The transition from the DB state to SD wave occurred when the glial capacity of K^+ uptake was completely depressed.

Our simulations suggest that varying the amplitude or duration of ES could trigger different states of neuronal excitability, which changes the dynamics of neuronal electrical behaviour. However, other parameters such as pulse width and frequency of stimulation are also important, for instance, a high frequency stimulation is usually applied to control Parkinsonian motor symptoms. Therefore, understanding the state transitions to these patterns and how ES interferes in this process would help to improve the electrical stimulation techniques to control different neurological disorders.

Acknowledgements

The authors thank FAPESP Grant 2011/211385 (G.F.), UNIEMP (B.S.M.) and CNPq Grant 309381/2012-6 (K.S.) for supporting this research.

References

1. M.D. Johnson, S. Miocinovic, C.C. McIntyre, J.L. Vitek, Neurother. J. Am. Soc. Exp. Neurother. **5**, 294 (2008)
2. G. Florence, M.A. Dahlem, A.-C.G. Almeida, J.W.M. Bassani, J. Kurths, J. Theor. Biol. **258**, 219 (2009)
3. M. Bikson, P.J. Hahn, J.E. Fox, J.G.R. Jefferys, J. Neurophysiol. **90**, 2402 (2003)
4. D. Bianchi, A. Marasco, A. Limongiello, C. Marchetti, H. Marie, B. Tirozzi, M. Migliore, J. Comput. Neurosci. **33**, 207 (2012)
5. A.A. Grace, J. Neural Transm. Suppl. **36**, 91 (1992).
6. A.A. Grace, B.S. Bunney, H. Moore, C.L. Todd, Trends Neurosci. **20**, 31 (1997)
7. O. Valenti, P. Cifelli, K.M. Gill, A.A. Grace, J. Neurosci. **31**, 12330 (2011)
8. T.J. McCown, R.S. Greenwood, G.D. Frye, G.R. Breese, Exp. Neurol. **86**, 527 (1984)
9. M.S. Jensen, Y. Yaari, J. Neurophysiol. **77**, 1224 (1997)
10. E.-H. Park, D.M. Durand, J. Theor. Biol. **238**, 666 (2006)
11. H. Kager, W.J. Wadman, G.G. Somjen, J. Comput. Neurosci. **22**, 105 (2007)
12. M. Bikson, J. Lian, P.J. Hahn, W.C. Stacey, C. Sciortino, D.M. Durand, J. Physiol. **531**, 181 (2001)
13. M. D. Johnson, C.C. McIntyre, J. Neurophysiol. **100**, 2549 (2008)
14. J.E. Rubin, D. Terman, J. Comput. Neurosci. **16**, 211 (2004)
15. C.H. Cline, S.S. Nair, D. Xu, J. Nair, B. Beitman, Conf. Proc. Annu. Int. Conf. IEEE Eng. Med. Biol. Soc. IEEE Eng. Med. Biol. Soc. Conf. **12**, 890 (2004)
16. K. Kömek, G. Bard Ermentrout, C.P. Walker, R.Y. Cho, Eur. J. Neurosci. **36**, 2146 (2012)
17. L. Øyehaug, I. Østby, C.M. Lloyd, S.W. Omholt, G.T. Einevoll, J. Comput. Neurosci. **32**, 147 (2012)
18. H. Kager, W.J. Wadman, G.G. Somjen, J. Neurophysiol. **84**, 495 (2000).
19. E.M. Izhikevich, *Dynamical Systems in Neuroscience: The Geometry of Excitability and Bursting* (The MIT Press, London, 2010)
20. D. Golomb, C. Yue, Y. Yaari, J. Neurophysiol. **96**, 1912 (2006)
21. M. Bazhenov, I. Timofeev, M. Steriade, T.J. Sejnowski, J. Neurophysiol. **92**, 1116 (2004)
22. B. Hille, *Ionic Channels of Excitable Membranes* (Sinaur Associates, Sunderland, 2001)
23. G. Florence, T. Pereira, J. Kurths, Commun. Nonlinear Sci. Numer. Simul. **17**, 4700 (2012)
24. M. Müller, G.G. Somjen, J. Neurophysiol. **83**, 735 (2000)
25. S. Chiken, A. Nambu, Front. Syst. Neurosci. **8**, 33 (2014)
26. B. Grafstein, J. Neurophysiol. **19**, 154 (1956)
27. A.P. Fertziger, J.B. Ranck Jr, Exp. Neurol. **26**, 571 (1970)
28. D.M. Durand, E.-H. Park, A.L. Jensen, Philos. Trans. R. Soc. Lond. B. Biol. Sci. **365**, 2347 (2010)
29. F. Fröhlich, M. Bazhenov, V. Iragui-Madoz, T.J. Sejnowski, Neurosci. Rev. J. Bringing Neurobiol. Neurol. Psychiatry **14**, 422 (2008)
30. F. Fröhlich, M. Bazhenov, Phys. Rev. E Stat. Nonlin. Soft Matter Phys. **74**, 031922 (2006)
31. A. Dovzhenok, A.S. Kuznetsov, PloS One **7**, e42811 (2012)
32. W. Walz, Neurochem. Int. **36**, 291 (2000)
33. H. Kager, W.J. Wadman, G.G. Somjen, J. Neurophysiol. **88**, 2700 (2002)
34. G.G. Somjen, H. Kager, W.J. Wadman, J. Comput. Neurosci. **25**, 349 (2008)